RSC Advances

This is an *Accepted Manuscript*, which has been through the Royal Society of Chemistry peer review process and has been accepted for publication.

Accepted Manuscripts are published online shortly after acceptance, before technical editing, formatting and proof reading. Using this free service, authors can make their results available to the community, in citable form, before we publish the edited article. This *Accepted Manuscript* will be replaced by the edited, formatted and paginated article as soon as this is available.

You can find more information about *Accepted Manuscripts* in the Information for Authors.

Please note that technical editing may introduce minor changes to the text and/or graphics, which may alter content. The journal's standard Terms & Conditions and the Ethical guidelines still apply. In no event shall the Royal Society of Chemistry be held responsible for any errors or omissions in this *Accepted Manuscript* or any consequences arising from the use of any information it contains.

ROYAL SOCIETY OF CHEMISTRY

www.rsc.org/advances

Journal Name

RSCPublishing

PAPER

Field emission properties of spinel $ZnCo_2O_4$ Microflowers

Cite this: DOI: 10.1039/x0xx00000x

Satyajit Ratha,[1] Ruchita T. Khare,[2] Mahendra A. More,[2] Ranjit Thapa,[3] Dattatray J. Late,[4,*] and Chandra Sekhar Rout[1,*]

Received 00th January 2012,
Accepted 00th January 2012

DOI: 10.1039/x0xx00000x

www.rsc.org/

Abstract: $ZnCo_2O_4$ microflowers were synthesized by a simple low temperature hydrothermal route. A single three-dimensional microflowers consists of hundreds of self-assembled petals, with a thickness of several nanometers. These microflowers have exceptionally thin edges with less no of petal layers. The $ZnCo_2O_4$ microflowers appeared to be stable and good field emitters.

RSC Advances Accepted Manuscript

1. Introduction

Recently, two-dimensional (2D) layered materials have attracted tremendous attention from the scientific community for their promising applications in field emission,[1,2] optoelectronics,[3,4] energy storage devices like supercapacitors,[5,6] lithium ion batteries,[7–9] solar cells[3] and sensing devices.[10,11] Field-emission is also known as Fowler-Nordheim tunneling, which is a form of quantum tunneling where electrons pass from an emitting cathode material (which is negatively biased) to the anode through a barrier (vacuum) in the presence of a high electric field.[12,13] This phenomenon is highly dependent both on the properties of the material and the shape of the particular cathode. The materials with higher aspect ratios and sharp edges produce higher field-emission currents.[1,2] 2D materials, including graphene,[14,15] metal oxides (ZnO, Co_3O_4),[16,17] chalcogenides such as MoS_2,[18] VS_2,[19,20] WS_2,[1] SnS_2,[2,21] CuS[22] and their hybrids including ZnO/graphene,[23] WS_2/graphene,[1] SnS_2/graphene,[2] VS_2/ZnO[20] and MoS_2/CNTs[24] etc. have been studied for field emission application.

Flower like structures are self-assembled 1D or 2D nanostructures having large proportions of numerous thin open edges, which make them a favorable material for field emission applications.[25–29] Aligned CNT flower arrays have been reported to act as a suitable low turn on field emission device due to better lateral emission from CNTs than from their top surface.[25,29] Graphene flowers exhibited enhanced field emission properties due to the electric field enhancement on the edges of the nano-slices and the sp^3-like defects on the surface of the nanocrystalline graphitic film.[26] Xu *et al*. reported field emission properties of ZnO flower structures with high emission current density and low turn-on field.[27] Report by Li *et al*. on the field emission performance of MoS_2 nanoflowers appeared to be superior with a current density of 0.01 and 10 mA/cm^2 at macroscopic field of 4.5–5.5 and 7.6–8.6 V/μm, respectively.[28] $ZnCo_2O_4$ (ZCO) is categorized into the group of compounds having a typical spinel structure. It is structurally similar to that of other simple spinels like $ZnCr_2O_4$, $MgAl_2O_4$, $ZnAl_2O_4$ etc. and belongs to the space symmetry group $Fd\bar{3}m \equiv O_h^7$. All the compounds in spinel category show a typical stoichiometry of the form AB_2O_4. Depending upon the different occupancy state of the interstices by the cations A^{2+} and B^{3+}, a spinel structure can either be a normal spinel or an inverse spinel.[30–34] A normal spinel has AB_2O_4 structure in which the divalent cations A^{2+} occupy the tetrahedral sites and the trivalent cations B^{3+} occupy all the octahedral sites. The anions (O^{2-}) tend to coordinate both the cations A^{2+} and B^{3+}, tetrahedrally and octahedrally respectively, forming a close packed FCC structure. A spinel unit-cell is made up of eight such FCC cells made by oxygen ions in the configuration 2×2×2 and it comprises of 32 oxygen atoms along with 8 A atoms (8a Wyckoff positions) and 16 B atoms (16d Wyckoff positions),[35–38] i.e. 24 cations in total. The same occurs in the case of an inverse spinel structure. However, in an inverse spinel structure, the tetrahedral sites are occupied by half of the trivalent cations (B^{3+}) and the octahedral sites are occupied by the other half of the trivalent cations (B^{3+}) as well as all of the divalent cations (A^{2+}) making a structure similar to the stoichiometric formula $B(BA)O_4$.[39,40] The ZCO compound reported here is a normal cubic spinel which consists of four tetrahedral primitive cells. The Zn^{2+} cations have higher affinity towards the tetrahedral lattice points, whereas Co^{3+} cations have more affinity towards octahedral lattice points as per the reported data.[36,41–43] Among all other spinel structured compounds such as $NiCo_2O_4$ and $MnCo_2O_4$, ZCO possesses more simple compositional changes during the incorporation of Zn^{2+} with Co_3O_4.[44] In this paper we report the growth of $ZnCo_2O_4$ flowers consisting of 2D nanosheets prepared by a simple low temperature hydrothermal route and their field emission properties were investigated for the first time.

2. Experimental

2.1. Chemicals

Zinc Nitrate hexahydrate ($Zn(NO_3)_2.6H_2O$, 99.5%), Cobalt Nitrate hexahydrate ($Co(NO_3)_2.6H_2O$, 97%) and Ethanol (analysis grade) were brought from Merck Specialities Private

Limited (India). Urea (CH_4N_2O, extrapure AR, 99.5%) was purchased from Sisco Research Laboratories Pvt. Ltd. (India). All the above chemicals were used as received without any kind of alteration. All the glasswares were cleaned thoroughly with aqua regia (highly oxidizing mixture solution containing concentrated HNO_3 and concentrated HCl in a volumetric ratio of 1:3) and thoroughly rinsed with DI water prior to usage.

2.2. Synthesis procedure for ZCO microflower structure

A low cost, low temperature hydrothermal route was followed for the synthesis of ZCO flower structures. Zinc and cobalt precursors were prepared from $Zn(NO_3)_2.6H_2O$ and $Co(NO_3)_2.6H_2O$ respectively. 3 mmol of $Zn(NO_3)_2.6H_2O$ and 6 mmol of $Co(NO_3)_2.6H_2O$ were first dissolved in 20 ml of DI water and then 60 mmol of urea (CH_4N_2O) was added to it under constant stirring condition. DI water was further added to the above solution to make the net volume, 60 ml. The solution was further stirred for about an hour and then it was transferred to a 100 ml borosilicate glass bottle and was kept at 90 °C in an oven for 12 hrs. After cooling the solution to room temperature, the slight purple colored precipitate was collected by centrifugation and it was washed repeatedly with DI water and ethanol to remove any impurity as well as unreacted ions. The as collected precipitate was further heated at 200 °C for 8 hrs to ward off any impure phase growth. The hydrothermal method comprises of various growth and nucleation stages in order to produce the final flower like structures. Also, we have carried out growth of ZnCo2O4 on different substrates such as glass, SiO_2/Si, ITO and ITO coated with ZnO seed layer (ZnO/ITO) to demonstrate possible ways of adhesion between the sample and substrates. From the experimental observation, it is found that the sample shows better bonding in case of ZnO/ITO in comparison to other substrates. ZCO on ITO/ZnO was characterized and the corresponding data can be found in the supplementary data.

2.3. Characterization and Field Emission studies

The shape, size and structure of ZCO were characterized by FESEM (MERLIN Compact with GEMINI I electron column, Zeiss Pvt. Ltd., Germany). Elemental analysis of the samples was carried out by EDAX analysis. Raman spectroscopy was performed by a micro Raman spectrometer (Renishaw inVia Raman microscope) with a laser excitation wavelength of 532 nm and laser power of 1 mW/cm^2. X-ray diffraction (XRD) patterns of the sample were obtained by a Bruker D8 Advanced diffractometer using Cu-Kα radiation (λ=1.54184 Å).

2.4. Theoretical calculations

Theoretical calculations were performed using density functional theory (DFT) as implemented in the CASTEP code.[45] Ultrasoft pseudopotentials were used to describe the core electrons.[46] The Perdew, Burke and Ernzerhof (**PBE**)[47] generalized gradient approximation (GGA) was employed for describing the exchange-correlation potentials. Brillouin zone sampling was made with the Monkhorst Pack scheme and a K-Point grid of 7x7x1. It was found that the cutoff energy of 400 eV is sufficient to give well-converged results. The structures were optimized until the total energy converged to less than 10^{-5}eV/atom and the maximum force converged to lower than 0.01 eV/Å. ZCO (111) was built by cleaving the geometrically optimized ZCO (space group $Fd\bar{3}m$) structure followed by further relaxation. Thus obtained ZCO (111) cell had lattice parameter of a = b = 8.101 Å, which is in good agreement with previously reported values.[48,49] A vacuum slab of length 20 Å was used in perpendicular direction to the ZCO (111) plane to ward off the spurious interactions with its own periodic image. The theoretical calculations results are summarized in Fig.1. The top and side view of optimised structure of (2x2) supercell of ZCO (111) surface are shown in Fig 1(a) and 1(b) respectively. Fig. 1(c) shows the electrostatic potential as a function of fractional coordinate for ZCO (111) surface. Considering the ZCO as stoichiometry, the work function has been estimated to be about 5.22 eV.

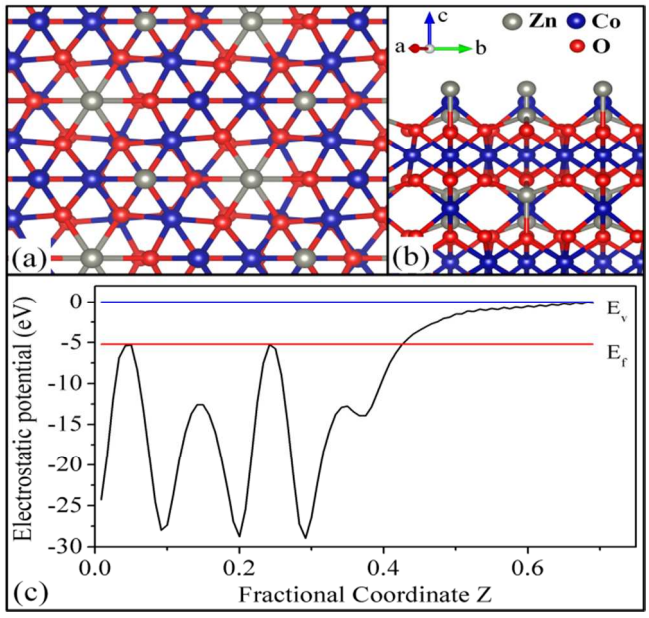

Fig. 1: **Optimized structure of $ZnCo_2O_4$(111) surface (a) top view and (b) side view, the zinc, cobalt and oxygen atoms are denoted with grey, blue and red balls respectively. The lattice parameter direction is indicated by the arrow shown in the inset of (b), the electrostatic potential along c-axis considering vacuum as reference energy is shown in (c). E_f and E_v correspond to the Fermi and vacuum energy.**

3. Results and discussion

3.1. Characterisation of the sample

Fig. 2 shows FESEM images of the sample at different reaction times. At reaction time of 0.5 hr (Fig. 2(a)), nanoparticles of Zn-Co-LDH are formed which become the platform for the nucleation and growth of the microspheres.[50,51] After reaction time of 1 hr (Fig. 2(b)), the nanoparticles aggregate in order to minimize their surface energy and form nanoflake like structures. The nanoflakes gradually grow in size and number to form microflakes as shown in Fig. 2(c). After 1.5 hrs orientation of those microflakes occurs due to crystallization and subsequently they form agglomerate (Fig. 2(d)) and after 2 hrs, the microflakes starts to grow in a highly ordered manner which initiates the growth of Zn-Co-LDH microflowers (Fig. 2(e) and 2(f)). The final product is further annealed at 200 °C for 8-10 hrs and as a result the Zn-Co-LDH composite oxidize and form highly crystalline ZCO microflowers with numerous edge growths. Fig. 3 shows the schematic of the mechanism on formation of ZCO microflowers in an illustrative way.

RSC Advances Accepted Manuscript

This journal is © The Royal Society of Chemistry 2012

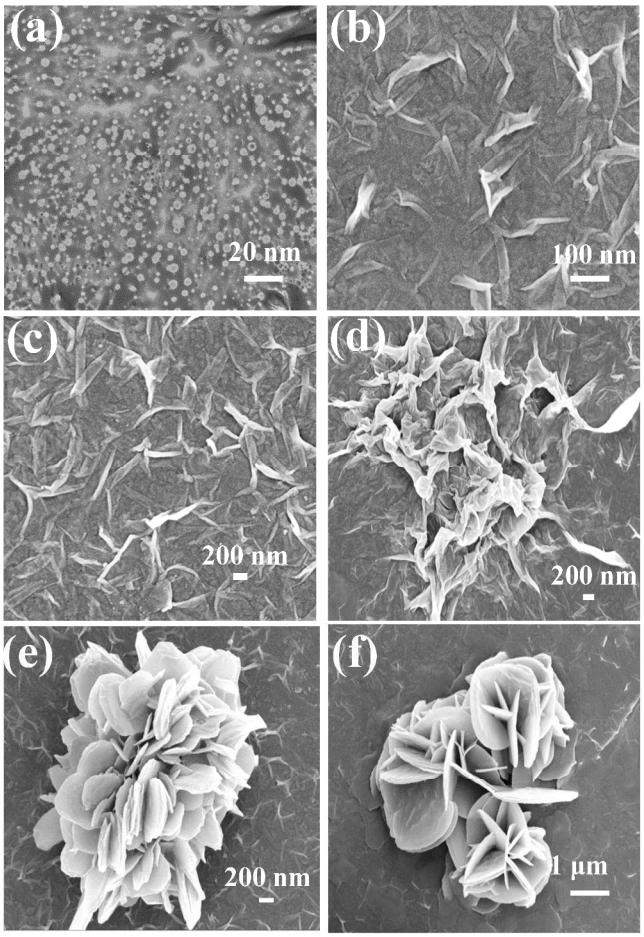

Fig.2: **FESEM images of the sample at different reaction times, (a) 0.5 hr, (b) 1 hr (high magnification), (c) 1 hr (low magnification), (d) 1.5 hrs, (e) and (f) 2 hrs.**

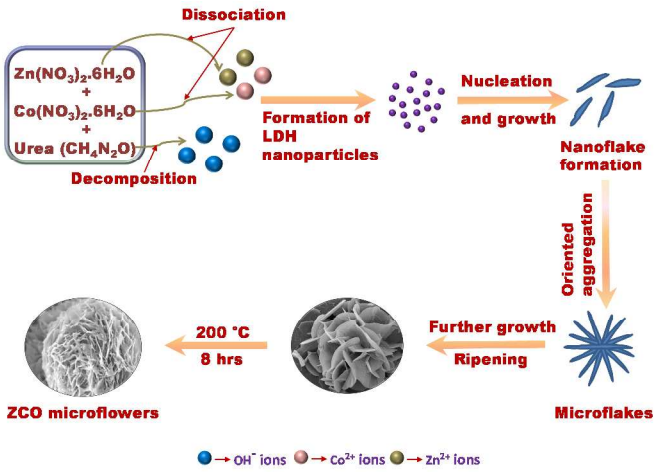

Fig.3: **Schematic interpretation of growth mechanism for ZCO flower structure.**

FESEM image (Fig.4a) shows uniform formation of ZCO microspheres.

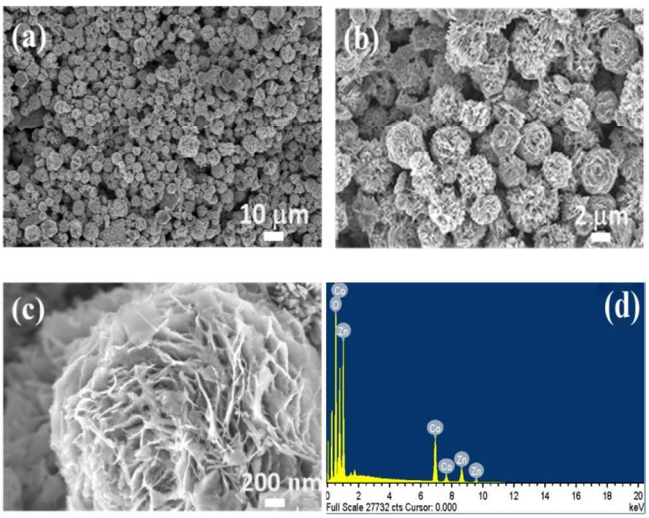

Fig.4: **FESEM images of spinel $ZnCo_2O_4$ flowers: (a) uniform formation of $ZnCo_2O_4$ flower-like microspheres and (b) an enlarged portion shows the 2D nanosheets which wrap up to form the spherical structure. (c) Further magnification reveals the thickness of the nanosheets which lies within the range ~20-30 nm. (d) EDS pattern of the ZCO sample.**

A magnified view of the sample (Fig.4b) reveals that the diameter of the microspherical structure is within the range of 6-10 µm. The structure is formed due to the wrapping up of ZCO nanoplates (Fig.4c) which have a thickness of the order of ~20-30 nm. The EDS pattern (Fig.4d) shows the peaks from all the three composing elements contained in the as prepared ZCO sample. Both Co and O show characteristic X-ray emission from their respective K-shells whereas in case of Zn, the X-ray emission occurs due to the electron returning to the L-shell. Table-1 shows the datasheet of EDS report in which the weight percentage and atomic percentage of all the three elements have been put and also the corresponding shells are shown inside the parentheses. It shows the presence of the elements in somewhat right proportions as expected considering the stoichiometric formula for ZCO. Both the weight percentage and atomic percentage are not 100% because of the presence of aluminium in traces and it constitutes the rest of the percentage. It occurred because the samples were prepared for EDS analyses on aluminium foils.

Table-1:

Element	Weight %	Atomic %
O (K)	24.17	54.33
Co (K)	43.35	27.45
Zn (L)	22.49	14.23

Fig.5 shows the typical TEM and HRTEM image of ZCO sample indicating highly crystalline nature of our sample. The lattice spacing and corresponding Miller indices are also being

RSC Advances Accepted Manuscript

denoted in the figure. Structure and morphology of the prepared ZCO sample was confirmed by XRD analysis. Fig.6 shows the XRD analysis of ZCO which indicates prominent growth along (311) direction. The diffraction peaks are attributed to the cubical spinel structured ZCO (JCPDS file: 23-1390).

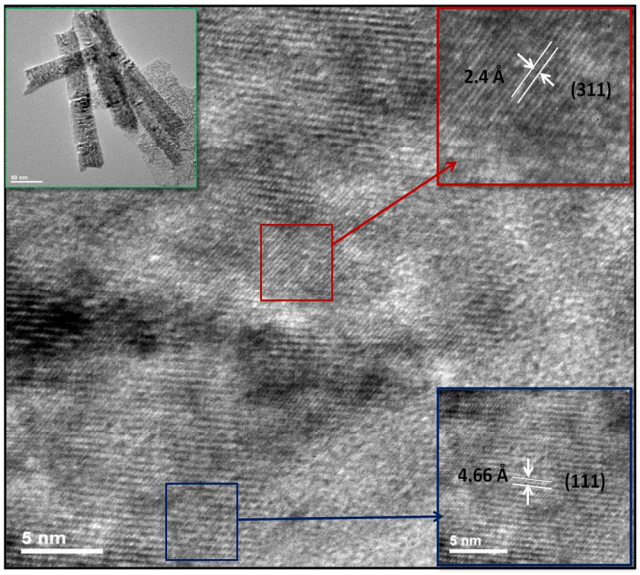

Fig. 5: TEM and HRTEM images of spinel $ZnCo_2O_4$ microflowers.

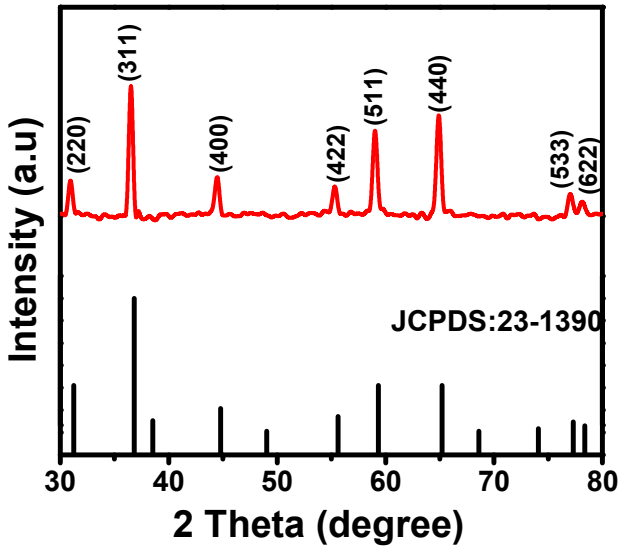

Fig.6: (a) XRD pattern of the ZCO sample

Though a typical spinel structure consists of 56 atoms in total, only 14 atoms are required to construct the simplest primitive cell structure. Therefore only 42 vibrational modes can be realized in this case. According to factor group analysis, there are 3 acoustic and 39 optical modes in a simple spinel like ZCO.[38,52] Thus Raman spectra (Fig.7) for the ZCO spinel can be distributed as follows.

The Raman band at 472 cm^{-1} corresponds to strong vibration due to the stretching of the bonds between Co-O and Zn-O to which the Raman active mode E_g can be assigned. The sharp band at 512 cm^{-1} corresponds to $F_{2g}^{(2)}$ mode which is due to the stretching of the Co-O bond. The peak at 610 cm^{-1} corresponds to $F_{2g}^{(1)}$ symmetry. The band at 682 cm^{-1} reveals the A_{1g} mode with a Raman shoulder peak at 658 cm^{-1} to which again the vibrational mode A_{1g} is assigned. Peaks from 610 cm^{-1} to 682 cm^{-1} corresponds to the Co-O bond stretching. All the peaks defined here are attributed to cubic spinel structured ZCO and other normal spinels which are structurally more or less similar to ZCO (such as $ZnCr_2O_4$) as illustrated in earlier reports.[38,53–61]

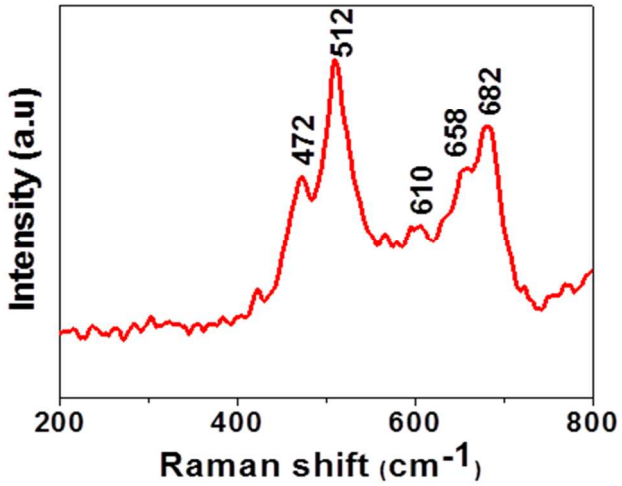

Fig.7: Raman spectra of spinel $ZnCo_2O_4$ flowers.

3.2. Field Emission properties of the sample

For field emission measurements, the $ZnCo_2O_4$ powder was sprinkled over carbon tape coated on a copper stub and loaded in a manner as to parallel phosphor coated conducting glass anode screen. The distance between the cathode and anode was manipulated by using a linear mechanical drive. Prior to readings, the emitters were kept at about 1KV for few minutes. The FE measurements were carried out inside a vacuum chamber at low pressure of about 2.8 x 10^{-8} Torr. The typical curve of the emission current density as a function of the applied field (J-E) plot is shown in Fig.8 (a). From the J-E plot the turn on field, defined as the field required to draw emission current density of 0.1μA/cm^2 is found to be 7.4 V/μm and the threshold field (which is defined as the applied field required to draw emission current density of 0.1mA/cm^2) is 12.2 V/μm. The corresponding F-N curve shown in Fig.8 (b) is observed to be non-linear. One of the parameters responsible for the nonlinear behavior of F-N plot is the 'effective' work function.

RSC Advances Accepted Manuscript

This journal is © The Royal Society of Chemistry 2012

It is believed that initially, when the applied field is low, the emitted electrons originate mainly from the conduction band

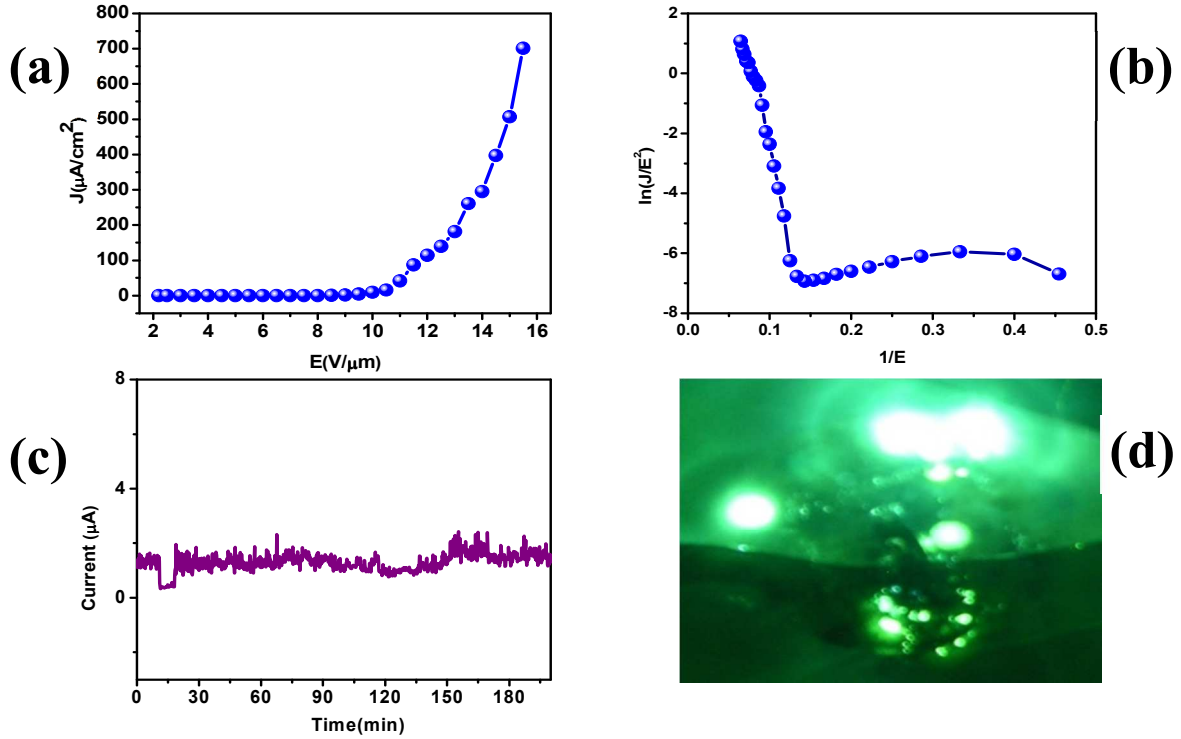

Fig.8: Field emission from spinel $ZnCo_2O_4$ flowers. (a) Applied electrical field as a function of emission current density. (b) F-N plot showing non-linear behavior indicating emission current from the semiconducting emitter. (c) Long term field emission current stability testing indicates fairly stable emission current. (d) Field emission image of the emitter operated at an electric field of 13.2 V/μm^{-1}

states, and as the applied field is increased, the valence band

electrons also tunnel out and contribute to the emission current. As the effective work function values for these two types of electrons (originating from CB and VB) are different, the F-N plot will show deviation from linearity. In addition, to this other factors such as field penetration, band bending, and screening also contributes to nonlinearity of the F-N plot.

The slope of the F–N plots has an inverse ratio to the field enhancement factor β and can be listed as follows

$$\beta = \frac{(-6.8\times10^{3})\phi^{3/2}}{m} \qquad (1)$$

On the basis of our DFT calculations, the work function of $ZnCo_2O_4$ microflower is 5.22 eV.

.

Emitter	Morphology	Synthesis method	Turn-on (V/μm)	Stability testing and fluctuations	Ref.
Co_3O_4	Nanowalls	Thermal evaporation	6	----------	62
ZnO	Nanowires	Vapor phase deposition	6	----------	63
ZnO	Nanotubes	Hydrothermal method	7	24h, <10%	64
ZnS	Nanowires	Vapor phase deposition	11.7	----------	65
$ZnCo_2O_4$	Microflowers	Hydrothermal method	7.4	3h, <5%	Present work

Table 2: Comparison of $ZnCo_2O_4$ field emitters with semiconducting nanostructures and nanocomposite

RSC Advances Accepted Manuscript

From the slopes of F–N plots the field enhancement factor β for $ZnCo_2O_4$ microflower obtained to be 6058. Along with the emission characteristics, the field emission current stability is one of the important parameters in the context of practical applications as a cold cathode. The current versus time (I–t) plots of $ZnCo_2O_4$ microflower recorded over the duration of 3 h is shown in Fig. 8(c) and it shows no obvious degradation of current density. Fig. 8(d) shows the field emission image of the emitters operated at an electric field of 13.2 $V\mu m^{-1}$. The light spots on the fluorescent screen are uniform and denser. Since the turn on field and threshold field both are dependent upon the contact performance, thus a better mechanical adhesion and electrical contact between microflowers and substrates will allow efficient electron injection, thereby reducing turn-on field and improving emission current density.

Table 2 depicts compilation of some semiconducting nanostructures and nanocomposites. As seen from the table 2, the present emitter ZCO exhibits comparable values of turn on and threshold fields.

Conclusions

In conclusion, $ZnCo_2O_4$ microflowers were synthesized for the first time by a simple low temperature hydrothermal route. Hundreds of petals self-assembled to form microflowers with exceptionally thin edges. This sharp edges microflowers proves to be a good field emitter with high aspect ratio for next generation field emission based devices.

Acknowledgements

R.T. Khare like to thank UGC BSR for fellowship. Dr. C.S. Rout and Dr. D. J. Late would like to thank DST (Government of India) for the Ramanujan fellowship. This work was supported by the DST-SERB Fast-track Young scientist (Grant No. SB/FTP/PS-065/2013), SB/FTP/PS-028/2013, SB/FT/CS-116/2013, Ramanujan Fellowship research grants (Grant No. SR/S2/RJN-21/2012, SR/S2/RJN-130/2012, UGC-UKIERI thematic awards (Grant No. UGC-2013-14/005), DST Nano-mission, CSIR-NCL-MLP project grant 028626 and the partial support by INUP IITB project sponsored by DeitY, MCIT, Government of India.

Notes and references

[a] [1]*School of Basic Sciences, Indian Institute of Technology,* Bhubaneswar *751013, India*

**Email: csrout@iitbbs.ac.in*

[2]*Department of Physics, University of Pune, Pune-411007, India*

[3]*SRM Research Institute, SRM University, Kattankulathur, Chennai 603203, Tamil Nadu, India*

[4]*Physical & Materials Chemistry Division, CSIR-National Chemical Laboratory, Dr. Homi Bhabha Road, Pashan, Pune 411008, India*

**Email:* dj.late@ncl.res.in / datta099@gmail.com

† Electronic Supplementary Information (ESI) available: [details of any supplementary information available should be included here]. See DOI: 10.1039/b000000x/

1. C. S. Rout, P. D. Joshi, R. V Kashid, D. S. Joag, M. A. More, A. J. Simbeck, M. Washington, S. K. Nayak, and D. J. Late, *Sci. Rep.*, 2013, **3**.

2. C. S. Rout, P. D. Joshi, R. V Kashid, D. S. Joag, M. A. More, A. J. Simbeck, M. Washington, S. K. Nayak, and D. J. Late, *Appl. Phys. Lett.*, 2014, **105**, 43109.

3. A. Dashora, U. Ahuja, and K. Venugopalan, *Comput. Mater. Sci.*, 2013, **69**, 216–221.

4. H. S. Lee, S.-W. Min, Y.-G. Chang, M. K. Park, T. Nam, H. Kim, J. H. Kim, S. Ryu, and S. Im, *Nano Lett.*, 2012, **12**, 3695–3700.

5. S. Ratha and C. S. Rout, *ACS Appl. Mater. Interfaces*, 2013, **5**, 11427–11433.

6. K.-J. Huang, L. Wang, Y.-J. Liu, Y.-M. Liu, H.-B. Wang, T. Gan, and L.-L. Wang, *Int. J. Hydrogen Energy*, 2013, **38**, 14027–14034.

7. C. Feng, L. Huang, Z. Guo, and H. Liu, *Electrochem. commun.*, 2007, **9**, 119–122.

8. J. Xiao, D. Choi, L. Cosimbescu, P. Koech, J. Liu, and J. P. Lemmon, *Chem. Mater.*, 2010, **22**, 4522–4524.

9. G. X. Wang, S. Bewlay, J. Yao, H. K. Liu, and S. X. Dou, *Electrochem. Solid-State Lett.*, 2004, **7**, A321–A323.

10. K. Ellmer, *Phys. status solidi*, 2008, **245**, 1745–1760.

11. A. Di Paola, L. Palmisano, M. Derrigo, and V. Augugliaro, *J. Phys. Chem. B*, 1997, **101**, 876–883.

12. G. N. Fursey, *Field emission in vacuum microelectronics*, Springer, 2007.

13. R. H. Fowler and L. Nordheim, *Proc. R. Soc. London. Ser. A, Contain. Pap. a Math. Phys. Character*, 1928, **119**, 173–181.

14. J. H. Deng, B. Yu, G. Z. Li, X. G. Hou, M. L. Zhao, D. J. Li, R. T. Zheng, and G. A. Cheng, *Nanoscale*, 2013, **5**, 12388–12393.

15. Q. Huang, G. Wang, L. Guo, Y. Jia, J. Lin, K. Li, W. Wang, and X. Chen, *Small*, 2011, **7**, 450–454.

16. P. Feng, X. Q. Fu, S. Q. Li, Y. G. Wang, and T. H. Wang, *Nanotechnology*, 2007, **18**, 165704.

17. T. Yu, Y. W. Zhu, X. J. Xu, Z. X. Shen, P. Chen, C. T. Lim, J. T. L. Thong, and C. H. Sow, *Adv. Mater.*, 2005, **17**, 1595–+.

18. R. V Kashid, D. J. Late, S. S. Chou, Y. K. Huang, M. De, D. S. Joag, M. A. More, and V. P. Dravid, *Small*, 2013, **9**, 2730–2734.

RSC Advances Accepted Manuscript

 This journal is © The Royal Society of Chemistry 2012

19. C. S. Rout, R. Khare, R. V Kashid, D. S. Joag, M. A. More, N. A. Lanzillo, M. Washington, S. K. Nayak, and D. J. Late, *Eur. J. Inorg. Chem.*, 2014, 5331–5336.

20. C. Q. Song, K. Yu, H. H. Yin, H. Fu, Z. L. Zhang, N. Zhang, and Z. Q. Zhu, *J. Mater. Chem. C*, 2014, **2**, 4196–4202.

21. H. X. Zhong, G. Z. Yang, H. W. Song, Q. Y. Liao, H. Cui, P. K. Shen, and C. X. Wang, *J. Phys. Chem. C*, 2012, **116**, 9319–9326.

22. X. P. Feng, Y. X. Li, H. B. Liu, Y. L. Li, S. Cui, N. Wang, L. Jiang, X. F. Liu, and M. J. Yuan, *Nanotechnology*, 2007, **18**, 145706.

23. W. T. Zheng, Y. M. Ho, H. W. Tian, M. Wen, J. L. Qi, and Y. A. Li, *J. Phys. Chem. C*, 2009, **113**, 9164–9168.

24. Q. F. Zhang, K. Yu, B. Zhao, Y. Wang, C. Q. Song, S. C. Li, H. H. Yin, Z. L. Zhang, and Z. Q. Zhu, *Rsc Adv.*, 2013, **3**, 10994–11000.

25. H. Kimura, B. Zhao, D. N. Futaba, T. Yamada, H. Kurachi, S. Uemura, and K. Hata, *Apl Mater.*, 2013, **1**, -.

26. J. C. Deng, L. Zhang, B. L. Zhang, and N. Yao, *Thin Solid Films*, 2008, **516**, 7685–7688.

27. F. Xu, K. Yu, G. D. Li, Q. Li, and Z. Q. Zhu, *Nanotechnology*, 2006, **17**, 2855–2859.

28. Y. B. Li, Y. Bando, and D. Golberg, *Appl. Phys. Lett.*, 2003, **82**, 1962–1964.

29. R. B. Sharma, D. J. Late, D. S. Joag, A. Govindaraj, and C. N. R. Rao, *Chem. Phys. Lett.*, 2006, **428**, 102–108.

30. S. D. Mo and W. Y. Ching, *Phys Rev B Condens Matter*, 1996, **54**, 16555–16561.

31. D. Bacorisen, R. Smith, and J. Ball, *Nucl. instruments …*, 2006, **250**, 36–45.

32. E. J. Palin and R. J. Harrison, *Mineral. Mag.* , 2007, **71** , 611–624.

33. S.-H. Wei and S. Zhang, *Phys. Rev. B*, 2001, **63**, 45112.

34. R. W. Grimes, A. B. Anderson, and A. H. Heuer, *J. Am. Chem. Soc.*, 1989, **111**, 1–7.

35. K. E. Sickafus, J. M. Wills, and N. W. Grimes, *J. Am. Ceram. Soc.*, 1999, **82**, 3279–3292.

36. E. J. W. Verwey and E. L. Heilmann, *J. Chem. Phys.*, 1947, **15**.

37. H. S. C. O'Neill and A. Navrotsky, *Am. Mineral.*, 1983, **68**, 181–194.

38. Z. V Marinković Stanojević, N. Romčević, and B. Stojanović, *J. Eur. Ceram. Soc.*, 2007, **27**, 903–907.

39. H. S. Mund, S. Tiwari, J. Sahariya, M. Itou, Y. Sakurai, and B. L. Ahuja, *J. Appl. Phys.*, 2011, **110**, -.

40. R. Hill, J. Craig, and G. V Gibbs, *Phys. Chem. Miner.*, 1979, **4**, 317–339.

41. A. Miller, *J. Appl. Phys.*, 1959, **30**, S24–S25.

42. D. S. McClure, *J. Phys. Chem. Solids*, 1957, **3**, 311–317.

43. J. D. Dunitz and L. E. Orgel, *J. Phys. Chem. Solids*, 1957, **3**, 318–323.

44. T. W. Kim, M. A. Woo, M. Regis, and K.-S. Choi, *J. Phys. Chem. Lett.*, 2014, **5**, 2370–2374.

45. M. D. Segall, J. D. L. Philip, M. J. Probert, C. J. Pickard, P. J. Hasnip, S. J. Clark, and M. C. Payne, *J. Phys. Condens. Matter*, 2002, **14**, 2717.

46. D. Vanderbilt, *Phys. Rev. B*, 1990, **41**, 7892–7895.

47. J. P. Perdew, K. Burke, and M. Ernzerhof, *Phys. Rev. Lett.*, 1996, **77**, 3865–3868.

48. Y. Sharma, N. Sharma, G. V Subba Rao, and B. V. R. Chowdari, *Adv. Funct. Mater.*, 2007, **17**, 2855–2861.

49. K. Krezhov and P. Konstantinov, *Acta Phys. Hungarica*, 1994, **75**, 243–246.

50. T. F. Hung, S. G. Mohamed, C. C. Shen, Y. Q. Tsai, W. S. Chang, and R. S. Liu, *Nanoscale*, 2013, **5**, 12115–12119.

51. M. Wang, T. Sun, Y. Shi, G. Jiang, and Y. Tang, *CrystEngComm*, 2014, **16**, 10624–10630.

52. P. Thibaudeau and F. Gervais, *J. Phys. Condens. Matter*, 2002, **14**, 3543.

53. S. Deng, R. Han, C. Dong, X. Xiao, J. Wu, and Y. Wang, *Mater. Lett.*, 2014, **134**, 138–141.

54. L. Saviot and D. B. Murray, *Phys. Rev. B*, 2009, **79**, 214101.

55. N. Combe and L. Saviot, *Phys. Rev. B*, 2009, **80**, 35411.

56. K. Samanta, P. Bhattacharya, R. Katiyar, W. Iwamoto, P. Pagliuso, and C. Rettori, *Phys. Rev. B*, 2006, **73**, 245213.

57. M. Tortosa, F. J. Manjón, M. Mollar, and B. Marí, *J. Phys. Chem. Solids*, 2012, **73**, 1111–1115.

58. C. M. Julien and M. Massot, *J. Physics-Condensed Matter*, 2003, **15**, 3151–3162.

59. C. M. Julien and M. Massot, *Mater. Sci. Eng. B-Solid State Mater. Adv. Technol.*, 2003, **97**, 217–230.

60. L. Malavasi, P. Galinetto, M. C. Mozzati, C. B. Azzoni, and G. Flor, *Phys. Chem. Chem. Phys.*, 2002, **4**, 3876–3880.

61. C. F. Windisch, G. J. Exarhos, and R. R. Owings, *J. Appl. Phys.*, 2004, **95**, 5435–5442.

RSC Advances Accepted Manuscript

62. C.-T. Hsieh, J.-M. Chen, H.-H. Lin, and H.-C. Shih, *Appl. Phys. Lett.*, 2003, **83**.

63. C. J. Lee, T. J. Lee, S. C. Lyu, Y. Zhang, H. Ruh, and H. J. Lee, *Appl. Phys. Lett.*, 2002, **81**.

64. A. Wei, X. W. Sun, C. X. Xu, Z. L. Dong, M. B. Yu, and W. Huang, *Appl. Phys. Lett.*, 2006, **88**, -.

65. Y. Chang, M. Wang, X. Chen, S. Ni, and W. Qiang, *Solid State Commun.*, 2007, **142**, 295–298.

RSC Advances Accepted Manuscript

 This journal is © The Royal Society of Chemistry 2012